Asian Journal of Andrology (2020) 22, 401–408
www.asiaandro.com; www.ajandrology.com

Open Access

ORIGINAL ARTICLE

Sperm Biology

Distribution of DNA damage in the human sperm nucleus: implications of the architecture of the sperm head

Silvia González-Rojo, Cristina Fernández-Díez, Marta Lombó, María Paz Herráez

The sperm nucleus is prone to sustain DNA damage before and after ejaculation. Distribution of the damage is not homogeneous, and the factors determining differential sensitivity among nuclear regions have not yet been characterized. Human sperm chromatin contains three structural domains, two of which are considered the most susceptible to DNA damage: the histone bound domain, harboring developmental related genes, and the domain associated with nuclear matrix proteins. Using a quantitative polymerase chain reaction (qPCR) approach, we analyzed the number of lesions in genes homeobox A3 (*HOXA3*), homeobox B5 (*HOXB5*), sex-determining region Y (SRY)-box 2 (*SOX2*), *β-GLOBIN, rDNA 18S*, and *rDNA 28S* in human sperm after ultraviolet irradiation (400 μW cm^{-2}, 10 min), H_2O_2 treatment (250 mmol l^{-1}, 20 min), and cryopreservation, which showed differential susceptibility to genetic damage. Differential vulnerability is dependent on the genotoxic agent and independent of the sperm nuclear proteins to which the chromatin is bound and of accessibility to the transcription machinery. Immunodetection of 8-hydroxy-2'-deoxyguanosine (8-OHdG) showed that the highest level of oxidation was observed after H_2O_2 treatment. The distribution of oxidative lesions also differed depending on the genotoxic agent. 8-OHdG did not colocalize either with histone 3 (H3) or with type IIα + β topoisomerase (TOPO IIα + β) after H_2O_2 treatment but matched perfectly with peroxiredoxin 6 (PRDX6), which is involved in H_2O_2 metabolism. Our study reveals that the characteristics of the sperm head domains are responsible for access of the genotoxicants and cause differential degree of damage to nuclear areas, whereas chromatin packaging has a very limited relevance. The histone-enriched genes analyzed cannot be used as biomarkers of oxidative DNA damage.

Asian Journal of Andrology (2020) **22**, 401–408; doi: 10.4103/aja.aja_26_19; published online: 14 June 2019

Keywords: biomarkers; DNA damage; human sperm; oxidative stress; sperm chromatin; sperm quality

INTRODUCTION

DNA damage in the male germline is an issue of a great concern with regard to causes of male infertility and to risks associated with the use of assisted reproductive technologies (ARTs). Chromatin is prone to suffer strand breaks and oxidative lesions during the process of spermatogenesis[1–4] and, subsequently, different factors such as aging, infections, radiation, and freezing/thawing can increase the range of DNA injuries in mature spermatozoa.[5–7] As reviewed by Aitken and Fisher[8], several studies have reported that sperm DNA damage, particularly reactive oxygen species (ROS)-mediated damage, is a main factor in the pathology of infertility. Oxidative stress, caused by ROS, is considered a major detrimental factor negatively affecting male fertility.[9,10] Excess ROS production promotes lipid peroxidation altering sperm parameters and causes DNA oxidative damage, which can lead to strand fragmentation.[5,11] Upon fertilization, the zygotic mechanisms of DNA repair are activated to correct failures of paternal origin,[12] but deleterious effects and transmission of mutations to the progeny can arise when the repairing ability is insufficient,[7,13] most *de novo* mutations (DNM) produced during fertilization being related to paternal, not maternal, inheritance.[13,14] Moreover, factors such as paternal age, also related to DNA integrity, have been related to the appearance in the male germline of DNM hotspots, whose distribution is not homogeneous in the genome.[15]

Distribution of chromatin lesions can be stochastic or it can preferentially affect particularly sensitive nuclear regions. Location of damage can be relevant when genes involved in the control of fertility and forthcoming development are affected. Moreover, the integrity of specific genes located in the injured area could represent a sensitive biomarker of genotoxic damage, more accurate than those methods (sperm chromatin structure assay [SCSA], terminal transferase dUTP nick end l abeling [TUNEL]) extensively used for DNA integrity evaluation in reproductive clinics, which offer global information about chromatin status.

Mammalian sperm chromatin displays three structural domains: (i) DNA bound to protamines configuring the toroids; (ii) DNA wrapped by histones in the nucleosomal regions, which represent 1%–15% of the mammalian genome;[16] and (iii) DNA attached to the sperm nuclear matrix (matrix attachment regions, MARs), linking toroids.[17,18] These protamine linker regions are nuclease sensitive and are presumed to harbor histones.[17,19] The first studies localized loci important for early development and imprinted genes in histone-bound DNA, the more accessible regions of chromatin.[16–18] These relaxed regions, histone enriched, have been postulated as more susceptible to

Department of Molecular Biology, Faculty of Biology, Universidad de León, Campus de Vegazana s/n León, León 24071, Spain.
Correspondence: Dr. MP Herráez (paz.herraez@unileon.es)
Received: 11 July 2018; Accepted: 03 January 2019

DNA damage.[20,21] This hypothesis, in particular with regard to sensitivity to oxidative damage, was strengthened by Noblanc and colleagues,[22] who colocalized the sperm nuclear basic protein, histone 3 (H3), and the nuclear matrix protein, type IIβ topoisomerase (TOPO IIβ), with 8-hydroxy-2'-deoxyguanosine (8-OHdG), in mouse spermatozoa. 8-OHdG is one of the more abundant forms of free radical-induced oxidative lesions, being widely used as a biomarker of oxidative DNA damage.[23] More recently, Kocer *et al*.[19] corroborated positional effects in two models of mice defective in antioxidant enzymes, some nuclear territories being more susceptible to the oxidative damage promoted during spermatogenesis. Their study on oxidative DNA immunoprecipitation and deep sequencing showed that vulnerability of the different chromosomes was independent of the persistence of nucleosomes or of their DNA methylation degree; some data suggested susceptibility of the inter-toroid DNA segments (MARs) and the short interspersed nuclear element (SINE) repeats (nonmethylated in mature spermatozoa). These studies on mice assessed oxidative damage before ejaculation in a mammalian model;[19,22] but mechanisms of DNA damage postejaculation could represent a different scenario.

The study of susceptibility to DNA damage in other species provides a wider perspective. In fish, the compaction pattern by sperm nuclear basic proteins (SNBPs) is completely different. Our group has demonstrated that, in rainbow trout and zebrafish spermatozoa (whose chromatin is totally packaged by protamines or histones, respectively), sensitivity to damage is independent of the SNBPs to which chromatin is bound.[24,25] The nuclear distribution of 8-OHdG and the study of the number of lesions in specific genes revealed that sensitive regions were different depending on the genotoxic agent, suggesting that other factors beyond the chromatin packaging were relevant to the accessibility of the genotoxicant to the DNA.

Our objective was to analyze the factors that render particular nuclear regions of mature spermatozoa more vulnerable to damage and to prove the hypothesis that histone H3-enriched areas, MAR regions, or early transcribed genes are more prone to injuries. Therefore, we analyzed the number of lesions promoted in different genes as well as the nuclear distribution of oxidative damage in human spermatozoa submitted to different treatments. The human sperm head includes a complex and regionalized system of enzymes controlling the redox reactions that are involved in the inactivation and distribution of ROS around the nucleus[26,27] and whose expression has never been related to DNA oxidative damage. The study of potential colocalization of oxidative damage within the sperm nucleus either with nuclear proteins or with enzymes involved in ROS metabolism will provide a better understanding of the relevance of nuclear and head architecture on the distribution of chromatin damage.

MATERIALS AND METHODS

Reagents

Unless otherwise indicated, all components used were purchased from Sigma (Sigma-Aldrich Spain, Madrid, Spain).

Sperm collection

Human sperm samples were obtained from young healthy men donors (25–30 years old, normozoospermic volunteers) by masturbation in accordance with the standards approved by the Research Ethics Committee of the University of León (León, Spain; #15 2013) and with 2010 WHO criteria.[28] All donors signed informed consent form. Ejaculates were maintained at 37°C and after liquefaction were processed within 1 h of extraction. A total of six different donors participated in the study, but only those samples which conformed with the following standards for volume (1.5 ml) and cell count (1.5×10^6 cells ml^{-1}) were selected; the specific number of samples used in each assay is indicated below. Sampling events took place over at least 1 week.

Exposure to damaging agents

Each semen sample was split into four aliquots to be subjected to different treatments: UV irradiation (254 nm, 400 μW cm^{-2}, 10 min at 15 cm from the lamp – Vilber, Eberhardzell, Germany), hydrogen peroxide (250 mmol l^{-1}, 20 min), and cryopreservation. Nontreated samples were used as control. After centrifugation (Sorvall™ Legend™ Micro 17R, Thermo Scientific, Waltham, MA, USA) at 1000 *g* for 5 min, seminal plasma was replaced with phosphate-buffered saline (PBS), and treatments were conducted at 37°C in a final volume of 1 ml (approximately 1×10^7–3×10^7 cells ml^{-1}). Cryopreservation was carried out following the procedure by Valcarce and colleagues.[29] Briefly, sperm samples were diluted 1:1 (*v*/*v*) in a commercial sperm freezing medium, equilibrated for 10 min at room temperature and loaded in 0.5 ml straws. The straws were placed in a horizontal rack at 2 cm above liquid nitrogen surface for 30 min and then were immersed and stored in liquid nitrogen until used. Thawing was performed at room temperature for 5 min. After each treatment, the samples were centrifuged at 2000 *g* for 5 min and washed with PBS. Oxidative stressed and cryopreserved samples were additionally washed with PBS to remove H_2O_2 or cryoprotectant remains.

Genomic DNA isolation

The pellets obtained after treatments were resuspended in 700 μl STE buffer (1% [*w*/*v*] sodium dodecyl sulfate [SDS], 10 mmol l^{-1} Tris-HCl pH 8.0, 1 mmol l^{-1} ethylenediamine tetraacetic acid [EDTA], 50 mmol l^{-1} NaCl), supplemented with 2 mg ml^{-1} proteinase K, and were incubated for 2 h at 55°C in a shaking bath. After proteinase K digestion, DNA was extracted using an optimized phenol: chloroform method described by González-Rojo and colleagues.[24]

DNA quantity and quality were determined by Nanodrop 1000 (Thermo Scientific, Wilmington, DE, USA) at 260 nm. Only high purity DNA (A_{260}/A_{280} >1.8) was used for the subsequent analysis.

Localization of genes in DNA fractions

The protocol described by Wykes and Krawetz[30] for the separation of histone- or protamine-bound DNA fractions (HDNA and PDNA, respectively) in human spermatozoa was applied using *Pvu*II as restriction endonuclease. Every 10^8 cells were washed twice with 4 ml TN buffer (25 mmol l^{-1} Tris-HCl, 100 mmol l^{-1} NaCl, pH 8.0) and centrifuged at 2000 *g* for 5 min. Cell pellets were resuspended in 1 ml TDTT buffer (50 mmol l^{-1} Tris-HCl, 10 mmol l^{-1} dithiothreitol [DTT], pH 8.0; freshly prepared) and incubated for 15 min on ice. After that, 10 μl 10% (*w*/*v*) cetyltrimethylammonium bromide was added (final concentration 0.1%) and incubation was for 30 min on ice. After centrifugation at 3000 *g* for 5 min at 4°C, the obtained pellets were resuspended in 1 ml TN buffer supplemented with 0.5% (*w*/*v*) digitonin and centrifuged again. This washing step was repeated five times. Nuclei pellets were resuspended in TNE buffer (10 mmol l^{-1} Tris-HCl, 0.65 mol l^{-1} NaCl, 1 mmol l^{-1} EDTA, pH 8.0) supplemented with 0.05% (*w*/*v*) digitonin and incubated for 15 min on ice. This incubation permitted extraction of the histone component which was recovered after centrifugation at 3000 *g* for 2 min at 4°C as supernatant. This supernatant was used for the histone purification as described in **Supplementary Materials and Methods** and **Supplementary Figure 1**. The nuclei pellet was subjected to digestion with 100 U of *Pvu*II in the enzyme buffer supplement with 0.05% digitonin for 1.5 h at 37°C. After digestion, the cleaved histone-enriched DNA (HDNA fraction) was recovered as supernatant after centrifugation at 3000 *g* for 2

min at 4°C. The pellet containing the PDNA fraction was resuspended in 1 ml STE buffer supplemented with 200 μg ml^{-1} proteinase K for gDNA extraction. Both tubes (corresponding to HDNA and PDNA fractions) were incubated at 50°C overnight and after that period the fractionated DNA was purified by a conventional phenol-chloroform protocol. Only the PDNA tube was again digested as described above and again purified by phenol-chloroform. The presumed HDNA and PDNA fractions were resuspended in TE buffer and were spectrophotometrically quantified at 260 nm. All fractions, including genomic DNA as control, were used for the conventional PCR amplification.

Localization of human genes in the HDNA or PDNA fractions was assessed by PCR in TGradient thermocycler (Biometra, Göttingen, Germany), with 25, 28, and 30 cycles of amplification. Each reaction was performed with samples obtained from three donors and technical replicates and nontemplate controls were included for each assay. Primers and conditions, as well as product amplification, are detailed below (**Table 1**, **Figure 1a** and **1b**).

Quantitative PCR

The method developed by Rothfuss and colleagues[31] was used as described by our group.[24,25,32] The basis of this approach is the delay of DNA polymerase when any alteration in DNA strand (strand breaks, abasic sites, pyrimidine dimers, *etc.*) appears, which is determined by quantitative PCR (qPCR). Amplification efficiency is proportional to the average frequency of lesions within a DNA region. Short amplicons (approximately 60 kb) are considered a virtually damage-free reference, whereas long amplicons (approximately 600 kb) display reduced efficiency according to the level of damage, so for each particular gene the ratio of the C_t value obtained in the qPCR for short and long amplicons permits calculation of lesion frequency (used to calculate the number of lesions per 10 kb).[33] qPCR was performed in triplicate on a StepOnePlus real-time thermal cycler (Applied Biosystems, Foster City, CA, USA) and a nontemplate control was used for each pair of primers. The number of lesions was studied in six genes: homeobox A3 (*HOXA3*), homeobox B5 (*HOXB5*), sex-determining region Y (SRY)-box 2 (*SOX2*), *β-GLOBIN*, *rDNA 18S*, and *rDNA 28S*. Primer design was carried out with Primer Express 2.0 software (Applied Biosystems). Amplification efficiency was determined for all nucleotides using serial dilutions of gDNA. PCR efficiencies were calculated with StepOnePlus version 2.2.2 (Applied Biosystems) using the linear regression slope of the dilution series (**Table 1**). Reaction conditions required 3 ng gDNA, except *SOX2* and *β-GLOBIN* genes, whose reactions needed 9 ng. Reaction conditions were a preincubation phase of 10 min at 95°C, followed by 50 cycles of 10 s at 95°C, 10 s at the annealing temperature (**Table 1**), and 50 s or 10 s (for long and short amplicons, respectively) at 72°C. Product specificity was verified by agarose gel electrophoresis (data not shown) and by melting curves and threshold cycles (C_ts), which were measured by StepOnePlus version 2.2.2 software.

The number of DNA lesions per 10 kb with respect to the basal level of lesions in nontreated samples was analyzed in each male independently and calculated according to the formula:[31]

$$Lesion\,rate = (1 - 2^{-(\Delta Ct\,long - \Delta Ct\,short)}) \times \frac{10000\,(bp)}{size\,of\,long\,fragment\,(bp)};$$

$$\Delta Ct = Ct\,(treated) - Ct\,(untreated)$$

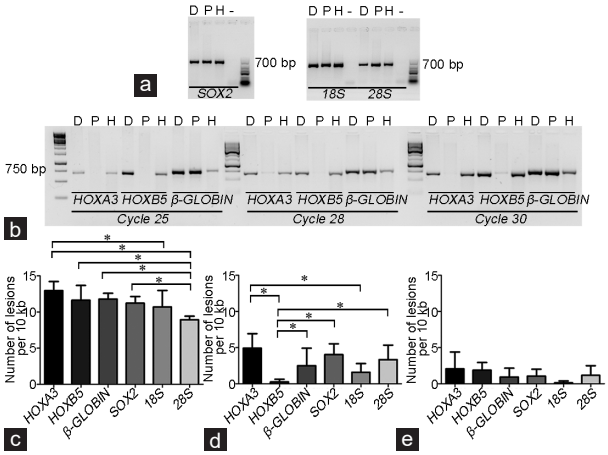

Figure 1: Location of genes in DNA fractions and quantification DNA lesions per 10 kb in human sperm. (**a**) Amplification of *SOX2*, *rDNA 18S,* and *rDNA 28S* human genes after chromatin fractionation. PCR was carried out with 30 cycles of amplification in triplicate. (**b**) Amplification of *HOXA3*, *HOXB5,* and *β-GLOBIN* after chromatin fractionation. PCR was carried out with 25, 28, and 30 cycles of amplification. Electrophoresis analysis was performed with PCR amplicons obtained from genomic DNA (lane D), digestion resistant DNA (PDNA enriched fraction [lane P]) and digestion sensitive DNA (HDNA enriched fraction [lane H]) (n = 3). Number of lesions in specific genes after (**c**) UV irradiation 400 μW cm^{-2}, 10 min, (**d**) H_2O_2 exposure 250 mmol l^{-1}, 20 min, or (**e**) cryopreservation, respect to the basal level of lesions in untreated samples. Data are expressed as mean ± standard deviation. $^*P < 0.05$, significant differences between the linked genes. *HOXA3*: homeobox A3; *SOX2*: sex-determining region Y (SRY)-box 2; *HOXB5*: homeobox B5; D: genomic DNA; P: protamine-enriched DNA; H: histone-enriched DNA; -: negative control; PCR: polymerase chain reaction.

Table 1: List of forward and reverse primers used in conventional polymerase chain reaction and quantitative polymerase chain reaction assays for human sperm samples

Genes GeneID	*Forward oligonucleotide (5'–3')*	*Reversed oligonucleotide (5'–3')*	*PCR product size (bp)*	*PCR efficiency (%)*	*Anneling temperature (°C)*
HOXA3	GAGGCTGTTGTCCGATAGGC	TCATACGGGACGCTGTTGAC	674	74.8	65
3200	GCGTGCAGATTTTTGGAGCA	GGATGCTTCGCGGTCTGTTA	60	102.9	58
HOXB5	TCTGACCCAGACTATCCCCA	GCCTCGCCTTGTGTTACGATA	679	93.1	65
3215	GACCCATCTCTCCCTTACCC	GCATCCACTCGCTCACTACA	60	109.4	58
SOX2	GACAGTTACGCGCACATGAA	TCCCCCAAAAAGAAGTCCAG	742	109.4	63
6657	CCACACTCACGCAAAAACCG	TCCCCCAAAAAGAAGTCCAGG	74	102.2	58
rDNA 18S	CGCGGTTCTATTTTGTTGGT	CGCTGAGCCAGTCAGTGTAG	672	103.2	63
JX132424.1	ATGGCCGTTCTTAGTTGGTG	ATGCCAGAGTCTCGTTCGTT	66	105.4	58
rDNA 28S	GCCGAAACGATCTCAACCTA	TGACCCATGTTCAACTGCTG	676	109.4	63
M11167.1	CTGCTCAGTACGAGAGGAACC	CAGCCAAGCACATACACCAA	55	102.9	58
β-GLOBIN	TGGTGCAAAGAGGCATGATA	GAAGGCTCATGGCAAGAAAG	750	105.6	63
3043	CCCTGTTACTTATCCCCTTCCT	GCTTGATGTTTTCTTTCCCCT	70	122.0	58

For all genes, their corresponding GenBank accession number is indicated, as well as the size of the amplicon, the oligonucleotide efficiency, and the annealing temperature. GeneID: GenBank accession number; bp: base pair; qPCR: quantitative polymerase chain reaction; *HOXA3*: homeobox A3; *SOX2*: sex determining region Y (SRY)-box 2; *HOXB5*: homeobox B5; PCR: polymerase chain reaction

Means ± standard deviations (s.d.; n = 4 different donors) were calculated (**Figure 1c–1e**).

TUNEL assay

DNA fragmentation was checked in smears in triplicate using a commercial kit (*In Situ* Cell Death Detection Kit, Fluorescein, Roche-Mannheim, Germany). The manufacturer's instructions were followed with slight modifications as is indicated in **Supplementary Information**. Data were expressed as the percentage of cells with fragmented DNA (mean ± s.d.; n = 3 different donors).

Immunolocalization of 8-OHdG

Samples were fixed with 4% (*w*/*v*) paraformaldehyde in PBS for 20 min at room temperature, washed three times with bi-distilled water, and diluted to a final concentration of 5×10^6 cells ml^{-1}. Next, 20 µl was smeared on (3-aminopropyl)triethoxysilane (ATE)-coated slides and left to desiccate at 37°C overnight. Nuclei were permeabilized with 0.1% (*v*/*v*) Triton-X 100 in 0.1% (*w*/*v*) sodium citrate, for 10 min at room temperature. The slides were washed twice in PBS for 10 min and blocked with 5% (*w*/*v*) bovine serum albumin (BSA) for 1 h at room temperature. Incubation with the primary antibody against 8-OHdG (dilution 1/200; ab62623, "anti-DNA/RNA damage antibody," Abcam, Cambridge, UK) continued overnight at 4°C and a negative control was included. Incubation with a Goat anti-Mouse secondary antibody labeled with orange-red AlexaFluor®568 (Life Technologies, Carlsbad, CA, USA) was at 37°C for 1 h. Nuclei were stained with 300 nmol l^{-1} 4',6-diamidino-2-phenylindole (DAPI) and the slides were mounted in ProLong® Gold Antifade Mountant (Thermo Scientific, Madrid, Spain). A negative control was included in the assay. Images were captured with a Zeiss LSM800 confocal microscope (Zeiss LSM800, Zeiss, Jena, Germany). To quantify the level of oxidation after treatments, at least 150 cells were analyzed per replicate with ImageJ software (Image J, Madison, WI, USA). Immunolocalization was carried out in four replicates in each donor sample (total of 600 cells per sample). The results were expressed as the percentage of cells with oxidized DNA (mean ± s.d.; n = 4 different donors) (**Figure 2a**). In addition, we quantified the percentage of oxidized cells showing a specific pattern of labeling, considering four possible distributions of the oxidative lesion: widespread across the nucleus, localized in an equatorial region, distributed over the subacrosomal and basal area, or localized at the basal region (**Figure 2b**). The results are expressed as the percentage of oxidized cells showing a specific distribution of 8-OHdG.

Colocalization of 8-OHdG with histone H3, TOPO IIα+β, and PRDX6

Double immunofluorescence of nontreated and H_2O_2-treated samples was performed following the protocol described above, modifying the primary antibody incubation. Primary antibody dilutions were: 1/200 mouse monoclonal 8-OHdG antibody (ab62623, "anti-DNA/RNA damage antibody," Abcam); 1/20 rabbit monoclonal TOPO IIα + β antibody (ab109524, Abcam); 1/200 rabbit polyclonal Histone H3 antibody (ab1791, Abcam); and 1/200 rabbit polyclonal PRDX6 antibody (ab59543, Abcam). Each specific antigen was revealed with a solution containing two secondary antibodies: Goat anti-Rabbit IgG (H+L) AlexaFluor®488 and Goat anti-Mouse IgG (H+L) AlexaFluor®568 (Life Technologies). Images were captured with a confocal microscope (**Figure 3**).

Statistical analyses

Statistical analysis was performed with SPSS version 21.0 (IBM, Chicago, IL, USA). A Shapiro–Wilk test was performed to check the normality of the data. When dealing with nonparametric data, a Kruskal–Wallis test was performed using the Dunn's *post hoc* test ($P < 0.05$). In the cases where the data behaved in a parametric form, an analysis of variance (ANOVA) with DMS *post hoc* test ($P < 0.05$) was carried out. The results are shown as mean ± s.d.

RESULTS

Different sensitivity to damage is revealed among the studied genes

Location of the studied genes was confirmed by agarose gel electrophoresis after HDNA/PDNA fractionation (**Figure 1a** and **1b**). *SOX2*, *18S,* and *28S* were distributed over the two fractions (**Figure 1a**). *HOXA3* and *HOXB5* genes appeared in HDNA, whereas the *β-GLOBIN* gene was located predominantly in protamine-enriched regions (**Figure 1b**). However, analysis of the number of lesions by qPCR, respect to the basal level of lesions in nontreated samples, did not correlate with the location of genes in histone- or protamine-enriched regions. The number of lesions in genes was significantly different depending on the treatment (**Figure 1c–1e**). UV irradiation caused the highest number of lesions, from 12.96 ± 1.26 (mean lesions per 10 kb DNA ± s.d.) for *HOXA3* to 8.93 ± 0.50 for *28S* (**Figure 1c**) with differences among genes. H_2O_2 treatment revealed a differential susceptibility among genes, with values obtained from 4.92 ± 2.01 for *HOXA3* to 0.26 ± 0.37 for *HOXB5* (both located in HDNA regions, as seen in **Figure 1d**). Differential sensitivity was subtler after cryopreservation, *HOXA3* being the most sensitive (2.07 ± 2.33) and *18S* the least (0.13 ± 0.26) (**Figure 1e**). None of the assayed treatments promoted a noticeable level of sperm DNA fragmentation with the TUNEL assay (**Supplementary Figure 2**).

8-OHdG localization is dependent on the genotoxic treatment

A basal rate of oxidation was detected in untreated samples (24.2% ± 1.7%, the percentage of cells with oxidized DNA); however, the highest level of oxidative damage was observed after H_2O_2 treatment (47.2% ± 7.0%; P = 0.015) (**Figure 2a**).

Moreover, the distribution of oxidative damage in the sperm head varies according to the treatment (**Figure 2b**). In untreated samples, little fluorescence was observed (**Figure 2b** and **2c**). After UV irradiation, most of the oxidized spermatozoa presented 8-OHdG throughout the subacrosomal region (48.9% ± 10.2%), others showing oxidation in the basal area (36.5% ± 9.9%) (**Figure 2b** and **2d**). In sharp contrast, H_2O_2 treatment promoted the appearance of 8-OHdG in an equatorial region (71.9% ± 9.5%), forming a well-defined peripheral band (**Figure 2b** and **2e**). After cryopreservation, a reduced number of cells were labeled, with mostly 8-OHdG restricted to the basal region of the nucleus, near the sperm neck (80.9% ± 4.7% of oxidized cells) (**Figure 2b** and **2f**).

8-OHdG colocalizes with PRDX6 but not with histone H3 or TOPO IIα+β

Distribution of histone H3 in human spermatozoon is restricted to the posterior area of the nucleus, close to the sperm neck, whereas TOPO IIα + β forms a subequatorial band around the nucleus (**Figure 3a**). After oxidative stress promoted by hydrogen peroxide, neither histone H3 nor TOPO IIα+β colocalized with the 8-OHdG pattern (**Figure 3b** and **3c**). PRDX6, involved in H_2O_2 metabolism, appeared in a different location in control cells and in cells treated with H_2O_2. In almost all the control cells, this enzyme appeared in the acrosomal area (**Figure 3a**), some cells showing traces in the intermediate segment. Treated cells showed PRDX6 located in the equatorial band colocalizing with 8-OHdG (**Figure 3d**) in almost all cases, but it was also seen to remain in the acrosome region in other cells (**Figure 3e**). In all cases, the presence of 8-OHdG perfectly matched the distribution of the enzyme (**Figure 3d** and **3e**). To rule out any fixative effect, or the inability of the antibody to reach the chromatin, we located the antigens

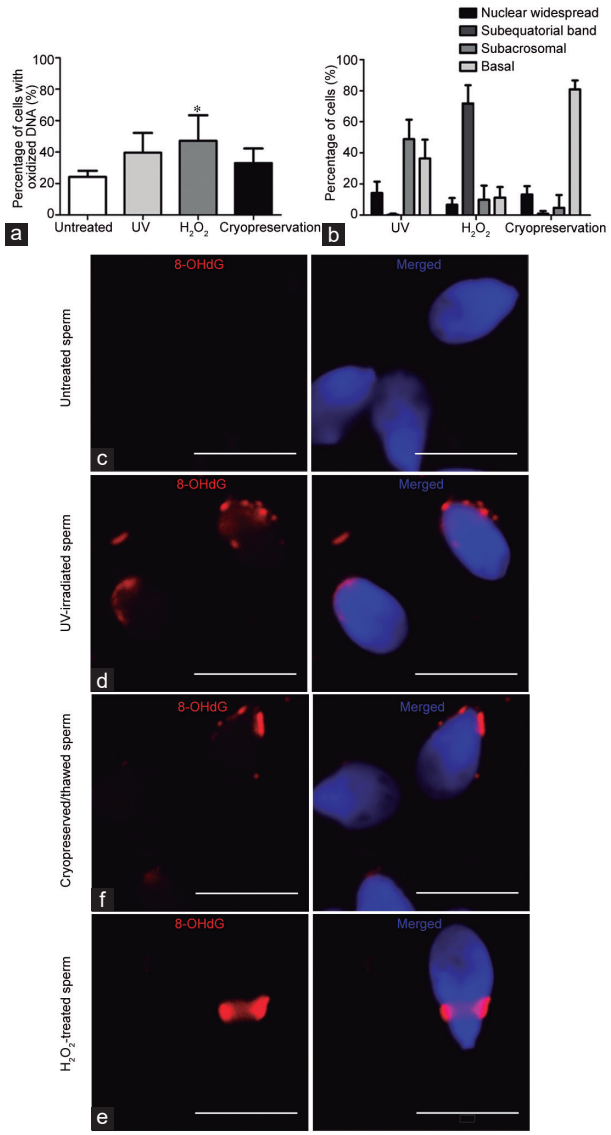

Figure 2: 8-OHdG localization in human sperm after treatments. (**a**) DNA oxidation is expressed as the percentage of cells with oxidized DNA. (**b**) The percentage of oxidized cells showing a specific pattern of 8-OHdG distribution was quantified. Data are expressed as mean ± standard deviation (n = 4, at least 150 cells were analyzed per replicate, total replicates: 4). Asterisk shows significant differences of treated samples respect to the untreated ones (P = 0.015). Representative confocal images were taken in (**c**) nontreated spermatozoa, (**d**) UV-irradiated samples, (**e**) H_2O_2-treated sperm, and (**f**) after cryopreservation, showing the location of 8-OHdG, labeled with AlexaFluor®568, in red fluorescence. Cell nuclei were stained with DAPI and are blue in color. Scale bars = 5 µm. UV: ultraviolete radiation; 8-OHdG: 8-hydroxy-2'-deoxyguanosine; DAPI: 4',6-diamidino-2-phenylindole.

with two immunofluorescence protocols which showed that distribution was identical to that described above (**Supplementary Figure 3**).

DISCUSSION

Sperm chromatin is vulnerable to different genotoxicants; several studies have reported positional effects that point to specific nuclear regions as potentially more sensitive.[19–22,29,34] In mammalian spermatozoa, the histone-associated DNA (nucleosomal regions or specific MARs), with a lower compacting degree, would be likely to accommodate the genes most susceptible to DNA damage caused during spermatogenesis and nuclear condensation.[20,22,29] Previous results from our group on rainbow

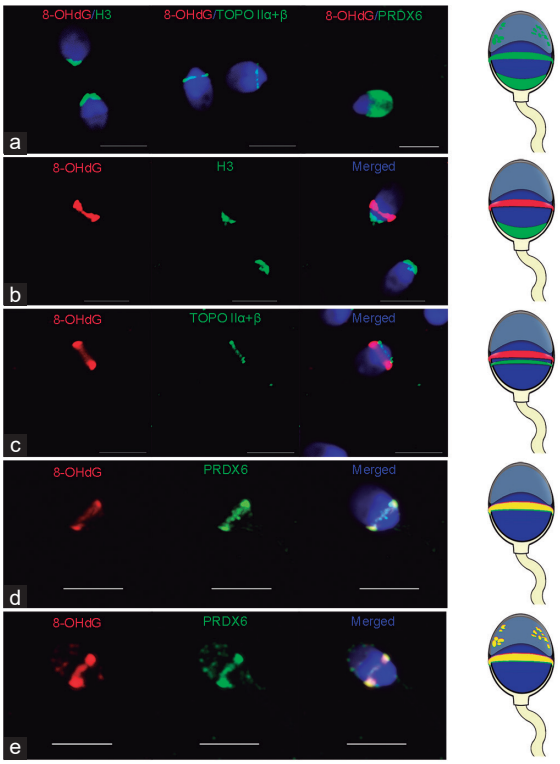

Figure 3: Distribution of 8-OHdG, histone H3, TOPO IIα + β, and PRDX6 in human sperm. Representative confocal images were taken of (**a**) untreated control spermatozoa and of (**b–e**) H_2O_2-treated sperm, showing the location of 8-OHdG labeled with AlexaFluor®568, in red fluorescence, and the distribution of (**b**) histone H3, (**c**) TOPO IIα + β and (**d** and **e**) PRDX6 labeled with AlexaFluor®488, green in color. Cell nuclei were stained with DAPI and appear in blue. Scale bars = 5 µm. Representative drawings outline the location of oxidative damage (red) and H3, TOPO IIα + β, and PRDX6 proteins (green) in human sperm nucleus (blue); colocation appears in yellow; acrosome appears in gray. 8-OHdG: 8-hydroxy-2'-deoxyguanosine; H3: histone 3; TOPO IIα + β: type IIα + β topoisomerase; PRDX6: peroxiredoxin 6; DAPI: 4',6-diamidino-2-phenylindole.

trout (*Oncorhynchus mykiss*) or zebrafish (*Danio rerio*) spermatozoa, homogeneously compacted with protamines or histones, respectively, have challenged the notion that histone regions are the most susceptible in mature spermatozoa. We demonstrated that, after ejaculation, differential susceptibility among nuclear regions was dependent on the type of harmful agent, rather than on the SNBPs the chromatin is bound to.[24,25] Moreover, Kocer and colleagues[19] linked the regions most sensitive to oxidative damage to chromosome positions in the mouse sperm nucleus. In the present study, data obtained with human spermatozoa, with nucleosomes at specific regulatory regions,[16,18] confirm our previous findings in other species with different sperm chromatin compaction.

The assayed treatments cause DNA damage by different mechanisms. UV irradiation has well-known effects on the DNA helix that result in fragmentation, formation of cyclobutane pyrimidine dimers (CPDs), and 2'-deoxyribonucleoside oxidation, specifically 8-OHdG.[35–37] Hydrogen peroxide, a ROS frequently used as a positive control of oxidative stress, promotes the formation of hydroxyl radicals upon reduction that lead to base oxidation and DNA strand fragmentation. Sperm cryopreservation, extensively used during ART, causes DNA fragmentation[7,38] and sperm chromatin decondensation[39] and generates ROS during the processes of freezing and thawing,[40–42] promoting oxidative DNA lesions, which have been confirmed after freezing/thawing in human spermatozoa.[43]

The selection of genes for lesion analysis was made in relation to their varying accessibility according to their association to SNBPs, epigenetic status, and relevance of early embryo development. The study of the human HDNA and PDNA fractions confirmed that human genes from the *HOX* cluster are located in nucleosome-enriched regions and, together with the *SOX2* gene (located in both fractions), display the epigenetic profile for early transcribed genes.[16,18,44] In contrast, the *β-GLOBIN* gene is protamine-enriched, is not located in histone-associated sites,[29,45] and is transcribed at later times. *18S* and *28S rDNA* are genes with a lower degree of accessibility.[46] According to the currently accepted hypothesis, *HOXA3*, *HOXB5*, and *SOX2* should be more susceptible to damage.

The results provided by the qPCR approach, which provides information on any kind of alteration in the analyzed genes and does not discriminate the type of lesion in the spot, clearly showed that the hypothesis was not verified. *HOXA*3 showed a greater sensitivity to UV than the ribosomal genes, the *28S* gene being the most resistant, but no differences among the rest of the analyzed genes, regardless of their particular association with SNBPs, were observed after irradiation. H_2O_2 treatment had a clear positional effect. *HOXA3* suffered more injuries than *HOXB*5 (both of them at the nucleosome region), but no more than *β-GLOBIN* (associated to protamines). Cryopreservation generated a low rate of lesions in the analyzed genes. The data given may suggest that the tested genotoxicants differentially affect human spermatozoa and that neither association with SNBPs nor presumed accessibility of genes to the transcription machinery may have a relevant role regarding higher susceptibility to damage. The assay of more target genes would be necessary to further support this hypothesis.

Assessment of the distribution of oxidative lesions by immunofluorescence provided further evidence. The anti-8-OHdG antibody has been recently validated to assess human sperm DNA oxidation.[23] However, the specific localization of 8-OHdG within the human sperm nucleus remains unclear. Untreated spermatozoa scarcely showed oxidative lesions. After UV irradiation, the vast majority of the cells were predominantly labeled in the subacrosomal or the basal region of the nucleus, the acrosomal area appearing to be more protected from damage. In the subacrosomal area, 8-OHdG did not remain peripheral but was observed at the inner part of the nucleus, revealing that UV penetrates deep into the genome. The content of the human acrosome may reduce UV penetration to the underlying nuclear region, because the UV absorption spectrum of the proteins is close to that of DNA. In contrast, after cryopreservation, most of the affected cells showed 8-OHdG in the basal area of the nucleus. ROS generation and oxidative stress are promoted during freezing/thawing.[47] Mitochondria, frequently cryodamaged, may be a localized source of ROS that could affect the closer nuclear territories. The presence of H3 in the basal area could also contribute to render this territory more unprotected.

H_2O_2 treatment, which promoted the highest rate of DNA oxidation, confirmed that association with SNBPs does not imply greater vulnerability of specific genes. The characteristic 8-OHdG pattern of labeling after H_2O_2 treatment of the human spermatozoon did not colocalize either with H3 or with TOPO IIα + β. Images are unequivocal: the oxidative lesions remain in an equatorial segment and the analyzed proteins were located in a more posterior region of the head. The study of the components of the antioxidant system responsible for H_2O_2 metabolism better explains the distribution of damage. H_2O_2 acts as a signaling molecule at physiological levels[26] and its diffusion across membranes is accomplished by specific peroxiporins.[48,49] In addition, spermatozoa possess a range of antioxidant enzymes including peroxiredoxins (PRDXs), which are direct targets for H_2O_2. PRDX4 has been identified in the plasma membrane, cytosol, and acrosome whereas PRDX1, PRDX5, and PRDX6 have been located in the equatorial segment of human spermatozoa.[27] PRDX6, the most abundant peroxiredoxin, is able to react with H_2O_2 at very low concentrations,[27] but at high H_2O_2 concentrations, it loses its detoxifying capacity. Our results show that PRDX6, commonly located at the acrosomal region, moves to the subequatorial area under oxidative stress, and that, in both locations, it perfectly colocalizes with 8-OHdG. Mobilization of the enzyme reveals a local requirement of its antioxidant activity, which could be generated by the equatorial location of particular peroxiporins guiding the H_2O_2 flow to the cell's interior.[27] Under physiological conditions, H_2O_2 rapidly reacts with PRDXs. In contrast, under pathological situations, such as the high concentration used in this study, PRDXs remain inactive, the spermatozoa being unprotected against H_2O_2 cytotoxic damage.[27] The specific location of peroxiporins and PRDXs and their activation/deactivation switch would seem to determine the exposure to H_2O_2 in the different head regions, the equatorial segment being particularly exposed to high H_2O_2 concentrations. This relationship is strengthened by those particular spermatozoa displaying an altered distribution of the enzyme, which always matches that of 8-OHdG, as is shown here (**Figure 4a**). Genes located in the vicinity of the equatorial segment could be the most susceptible to injuries caused by H_2O_2. According to Manvelyan and coworkers,[50] the *HOXB5* gene is accommodated in chromosome 17, which is located in the central area of the nuclei, which may explain the lower number of lesions detected by qPCR in this gene after H_2O_2 treatment. In addition, the *HOXA3*,

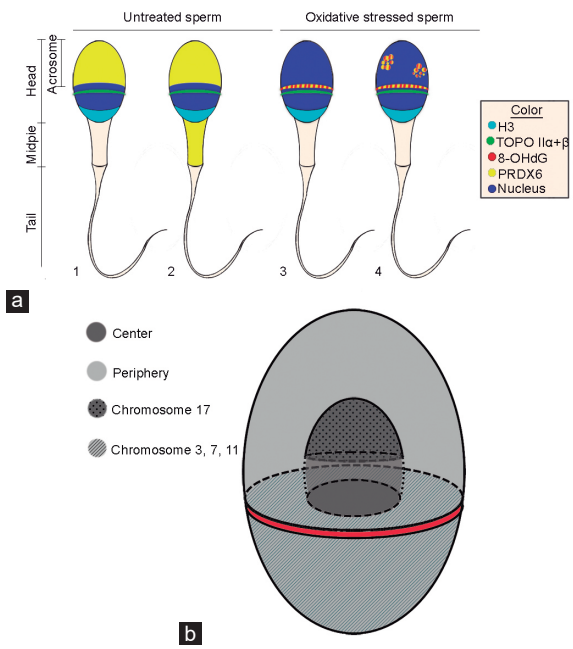

Figure 4: (**a**) Distribution of chromatin oxidative damage, the nuclear proteins H3 and TOPO IIα+β, and the antioxidant enzyme PRDX6 in human sperm. Distribution of 8-OHdG and the analyzed proteins in untreated and H_2O_2-treated sperm is summarized. Two patterns are shown in each condition, the normal distribution (1, 3) and the eventual pattern displayed by a reduced number of cells (2, 4). (**b**) Human sperm nucleus representation, following Manvelyan *et al.*'s description.[50] Dark gray shows the center area of the nucleus, and light gray the periphery. In addition, the drawing highlights the potential distribution of chromosome 17 (dark gray with dots) and chromosomes 3, 7, and 11 (light gray with crosswise lines). 8-OHdG: 8-hydroxy-2'-deoxyguanosine; H3: histone 3; TOPO IIα+β: type IIα+β topoisomerase; PRDX6: peroxiredoxin 6.

SOX2, and *β-GLOBIN* genes, revealed as very sensitive to the H_2O_2 treatment by the qPCR approach, are located in chromosomes 7, 11, and 3, respectively, which are located in the peripheral and equatorial region of the sperm nucleus (**Figure 4b**).

Location of damage has further implications with regard to reproductive performance. The paternal inheritance of DNM through the male germline has been shown to be linked to several diseases such as Alexander disease,[51] Crouzon, Noona, and Pfeiffer syndromes[52] or several neurodevelopmental disorders (reviewed[15]). The potential location of genes in the nuclear areas most sensitive to a particular stress could increase the chances of paternal transmission of specific syndromes.

Our results demonstrate that differences in sensitivity to DNA damage could be due to the head and the nuclear architecture, which influence the accession of genotoxicants to certain nuclear territories. Chromatin compaction or epigenetic status could be a secondary, less significant barrier. Considering that nuclear distribution of the damage caused by H_2O_2 does not mimic that promoted by other damaging agents, its use for the study of the effects of oxidative stress in sperm should be carefully considered.

CONCLUSIONS

We conclude that genes located in nucleosomal regions of human sperm nuclei do not show higher susceptibility to injury. DNA oxidative damage presents positional effects related to the nature of the damaging agent, the structural characteristics of the sperm head, and the physiological differences between head domains, driving their access to different nuclear territories. The identification of particular genes that could serve as sensitive biomarkers of DNA damage applied to clinical practices should be specific for the genotoxicant.

AUTHOR CONTRIBUTIONS

SGR performed experiments, analyzed results, designed the graphical representations, and wrote the manuscript; CFD and ML helped perform experiments, collaborated with the interpretation of data and reviewed the manuscript; MPH conceived and designed experiments, was responsible for the project, critical discussion, and interpretation of results and wrote and reviewed the manuscript. All authors read and approved the final manuscript.

COMPETING INTERESTS

All authors declared no competing interests.

ACKNOWLEDGMENTS

This work was supported by the Spanish Ministry of Economy and Competitiveness (project AGL2011-27787; AGL2014-53167-C3-3-R), Junta de Castilla y León (Spain) (EDU/1083/2013) and Fondo Social Europeo.

Supplementary Information is linked to the online version of the paper on the *Asian Journal of Andrology* website.

REFERENCES

1 Fujii J, Imai H. Redox reactions in mammalian spermatogenesis and the potential targets of reactive oxygen species under oxidative stress. *Spermatogenesis* 2014; 4: e979108.
2 Sakkas D, Bizzaro D, Manicardi GC. Chromatin damage and male infertility. In: Carrell DT, editor. The Genetics of Male Infertility. Totowa: Humana Press; 2007. p303–15.
3 De Vries M, Ramos L, Housein Z, De Boer P. Chromatin remodelling initiation during human spermiogenesis. *Biol Open* 2012; 1: 446–57.
4 Gunes S, Al-Sadaan M, Agarwal A. Spermatogenesis, DNA damage and DNA repair mechanisms in male infertility. *Reprod Biomed Online* 2015; 31: 309–19.
5 Aitken RJ, De Iuliis GN. On the possible origins of DNA damage in human spermatozoa. *Mol Hum Reprod* 2010; 16: 3–13.
6 Aitken RJ, Koppers AJ. Apoptosis and DNA damage in human spermatozoa. *Asian J Androl* 2011; 13: 36–42.
7 Herráez MP, Ausió J, Devaux A, González-Rojo S, Fernández-Díez C, *et al*. Paternal contribution to development: sperm genetic damage and repair in fish. *Aquaculture* 2017; 472: 45–59.
8 Aitken J, Fisher H. Reactive oxygen species generation and human spermatozoa: the balance of benefit and risk. *Bioessays* 1994; 16: 259–67.
9 Lewis SE, Aitken RJ. DNA damage to spermatozoa has impacts on fertilization and pregnancy. *Cell Tissue Res* 2005; 322: 33–41.
10 Bisht S, Dada R. Oxidative stress: major executioner in disease pathology, role in sperm DNA damage and preventive strategies. *Front Biosci (Schol Ed)* 2017; 9: 420–47.
11 Zribi N, Chakroun NF, Elleuch H, Abdallah FB, Ben Hamida AS, *et al*. Sperm DNA fragmentation and oxidation are independent of malondialdheyde. *Reprod Biol Endocrinol* 2011; 9: 47.
12 Fernández-Díez C, González-Rojo S, Montfort J, Le Cam A, Bobe J, *et al*. Inhibition of zygotic DNA repair: transcriptome analysis of the offspring in trout (*Oncorhynchus mykiss*). *Reproduction* 2014; 149: 101–11.
13 Marchetti F, Bishop J, Gingerich J, Wyrobek AJ. Meiotic interstrand DNA damage escapes paternal repair and causes chromosomal aberrations in the zygote by maternal misrepair. *Sci Rep* 2015; 5: 7689.
14 Kong A, Frigge ML, Masson G, Besenbacher S, Sulem P, *et al*. Rate of *de novo* mutations and the importance of father's age to disease risk. *Nature* 2012; 488: 471–5.
15 Girard SL, Bourassa CV, Lemieux Perreault LP, Legault MA, Barhdadi A, *et al*. Paternal age explains a major portion of *de novo* germline mutation rate variability in healthy individuals. *PLoS One* 2016; 11: e0164212.
16 Brykczynska U, Hisano M, Erkek S, Ramos L, Oakeley EJ, *et al*. Repressive and active histone methylation mark distinct promoters in human and mouse spermatozoa. *Nat Struct Mol Biol* 2010; 17: 679–87.
17 Ward WS. Function of sperm chromatin structural elements in fertilization and development. *Mol Hum Reprod* 2010; 16: 30–6.
18 Hammoud SS, Nix DA, Zhang H, Purwar J, Carrell DT, *et al*. Distinctive chromatin in human sperm packages genes for embryo development. *Nature* 2009; 460: 473–8.
19 Kocer A, Henry-Berger J, Noblanc A, Champroux A, Pogorelcnik R, *et al*. Oxidative DNA damage in mouse sperm chromosomes: size matters. *Free Radic Biol Med* 2015; 89: 993–1002.
20 Champroux A, Torres-Carreira J, Gharagozloo P, Drevet JR, Kocer A. Mammalian sperm nuclear organization: resiliencies and vulnerabilities. *Basic Clin Androl* 2016; 26: 17.
21 Miller D, Brinkworth M, Iles D. Paternal DNA packaging in spermatozoa: more than the sum of its parts? DNA, histones, protamines and epigenetics. *Reproduction* 2010; 139: 287–301.
22 Noblanc A, Damon-Soubeyrand C, Karrich B, Henry-Berger J, Cadet R, *et al*. DNA oxidative damage in mammalian spermatozoa: where and why is the male nucleus affected? *Free Radic Biol Med* 2013; 65: 719–23.
23 Vorilhon S, Brugnon F, Kocer A, Dollet S, Bourgne C, *et al*. Accuracy of human sperm DNA oxidation quantification and threshold determination using an 8-OHdG immuno-detection assay. *Hum Reprod* 2018; 33: 553–62.
24 González-Rojo S, Fernández-Díez C, Guerra SM, Robles V, Herraez MP. Differential gene susceptibility to sperm DNA damage: analysis of developmental key genes in trout. *PLoS One* 2014; 9: e114161.
25 González-Rojo S, Fernández-Díez C, Lombó M, Herráez MP. Distribution of DNA damage in the sperm nucleus: a study of zebrafish as a model of histone-packaged chromatin. *Theriogenology* 2018; 122: 109–15.
26 O'Flaherty C. The enzymatic antioxidant system of human spermatozoa. *Adv Androl* 2014; 2014: 1–15.
27 O'Flaherty C. Peroxiredoxins: hidden players in the antioxidant defence of human spermatozoa. *Basic Clin Androl* 2014; 24: 4.
28 Worl Health Organization. WHO Laboratory Manual for the Examination and Processing of Human Semen. 5th ed. Geneva: World Health Organization; 2010.
29 Valcarce DG, Cartón-García F, Riesco MF, Herráez MP, Robles V. Analysis of DNA damage after human sperm cryopreservation in genes crucial for fertilization and early embryo development. *Andrology* 2013; 1: 723–30.
30 Wykes SM, Krawetz SA. The structural organization of sperm chromatin. *J Biol Chem* 2003; 278: 29471–7.
31 Rothfuss O, Gasser T, Patenge N. Analysis of differential DNA damage in the mitochondrial genome employing a semi-long run real-time PCR approach. *Nucleic Acids Res* 2010; 38: e24.
32 Riesco MF, Robles V. Cryopreservation causes genetic and epigenetic changes in zebrafish genital ridges. *PLoS One* 2013; 8: e67614.
33 Zhu S, Coffman JA. Simple and fast quantification of DNA damage by real-time PCR, and its application to nuclear and mitochondrial DNA from multiple tissues of aging zebrafish. *BMC Res Notes* 2017; 10: 269.
34 Arpanahi A, Brinkworth M, Iles D, Krawetz SA, Paradowska A, *et al*. Endonuclease-sensitive regions of human spermatozoal chromatin are highly enriched in promoter and CTCF binding sequences. *Genome Res* 2009; 19: 1338–49.
35 Schuch AP, Menck CF. The genotoxic effects of DNA lesions induced by artificial UV-radiation and sunlight. *J Photochem Photobiol B Biol* 2010; 99: 111–6.

36 Epe B. DNA damage spectra induced by photosensitization. *Photochem Photobiol Sci* 2012; 11: 98–106.
37 Kawanishi S, Hiraku Y, Oikawa S. Mechanism of guanine-specific DNA damage by oxidative stress and its role in carcinogenesis and aging. *Mutat Res* 2001; 488: 65–76.
38 Tatone C, Di Emidio G, Vento M, Ciriminna R, Artini PG. Cryopreservation and oxidative stress in reproductive cells. *Gynecol Endocrinol* 2010; 26: 563–7.
39 Boitrelle F, Albert M, Theillac C, Ferfouri F, Bergere M, *et al*. Cryopreservation of human spermatozoa decreases the number of motile normal spermatozoa, induces nuclear vacuolization and chromatin decondensation. *J Androl* 2012; 33: 1371–8.
40 Thomson LK, Fleming SD, Aitken RJ, De Iuliis GN, Zieschang JA, *et al*. Cryopreservation-induced human sperm DNA damage is predominantly mediated by oxidative stress rather than apoptosis. *Hum Reprod* 2009; 24: 2061–70.
41 Zribi N, Chakroun NF, Ben Abdallah F, Elleuch H, Sellami A, *et al*. Effect of freezing–thawing process and quercetin on human sperm survival and DNA integrity. *Cryobiology* 2012; 65: 326–31.
42 Peris SI, Bilodeau JF, Dufour M, Bailey JL. Impact of cryopreservation and reactive oxygen species on DNA integrity, lipid peroxidation, and functional parameters in ram sperm. *Mol Reprod Dev* 2007; 74: 878–92.
43 Zribi N, Feki Chakroun N, El Euch H, Gargouri J, Bahloul A, *et al*. Effects of cryopreservation on human sperm deoxyribonucleic acid integrity. *Fertil Steril* 2010; 93: 159–66.
44 Hammoud SS, Purwar J, Pflueger C, Cairns BR, Carrell DT. Alterations in sperm DNA methylation patterns at imprinted loci in two classes of infertility. *Fertil Steril* 2010; 94: 1728–33.
45 Gardiner-Garden M, Ballesteros M, Gordon M, Tam PP. Histone- and protamine-DNA association: conservation of different patterns within the beta-globin domain in human sperm. *Mol Cell Biol* 1998; 18: 3350–6.
46 Wu SF, Zhang H, Cairns BR. Genes for embryo development are packaged in blocks of multivalent chromatin in zebrafish sperm. *Genome Res* 2011; 21: 578–89.
47 Makarova NP, Romanov YA, Dolgushina NV, Parker MM, Krasnyi AM. Comparative analysis of the expression of glutathione peroxidase and glutathione reductase genes in human sperm after cryopreservation. *Bull Exp Biol Med* 2018; 165: 166–70.
48 Bienert GP, Chaumont F. Aquaporin-facilitated transmembrane diffusion of hydrogen peroxide. *Biochim Biophys Acta* 2014; 1840: 1596–604.
49 Sies H. Role of metabolic H_2O_2 generation: redox signaling and oxidative stress. *J Biol Chem* 2014; 289: 8735–41.
50 Manvelyan M, Hunstig F, Bhatt S, Mrasek K, Pellestor F, *et al*. Chromosome distribution in human sperm – a 3D multicolor banding-study. *Mol Cytogenet* 2008; 1: 25.
51 Li R, Johnson AB, Salomons GS, van der Knaap MS, Rodriguez D, *et al*. Propensity for paternal inheritance of *de novo* mutations in Alexander disease. *Hum Genet* 2006; 119: 137–44.
52 Glaser RL, Jiang W, Boyadjiev SA, Tran AK, Zachary AA, *et al*. Paternal origin of FGFR2 mutations in sporadic cases of Crouzon syndrome and Pfeiffer syndrome. *Am J Hum Genet* 2000; 66: 768–77.

SUPPLEMENTARY MATERIALS AND METHODS

Histone purification

Extraction of histones was confirmed by Dot blot analysis (**Supplementary Figure 2**). The supernatant obtained after histone extraction was mixed with 0.4 N HCl (final concentration) and incubated at 4°C overnight. After centrifugation at 16 000 *g* for 10 min at 4°C, TCA was added to the supernatant to a final concentration of 33% (v/v) and incubated at 4°C overnight. The tubes were centrifuged 16 000 *g* for 15 min at 4°C and the pellet was resuspended in 1 ml of cold acetone. Centrifugation at 16 000 *g* for 5 min at 4°C was carried out and the pellet was washed twice with cold acetone. Finally, the obtained pellet was solubilized in a buffer containing 8 M urea and 4% (w/v) SDS and stored at −20°C until its use. For Dot blot analysis, histones from the human sperm samples and from commercial calf thymus (2 µl) were used. Nitrocellulose membrane was blocked in 3% (w/v) nonfat milk, 0.2% (v/v) Tween-20 in Tris-buffered saline (TBS-T) for 1 h at room temperature. Primary antibody incubation was prolonged overnight at 4°C using a rabbit polyclonal antibody against Histone H3 (dilution 1/8000) (ab1791, Abcam, Cambridge, UK). Primary antibody was labeled with secondary anti-rabbit antibody conjugated with horseradish peroxidase using a 1/10 000 dilution and was developed using the Pierce ECL substrate.

TUNEL asssay

Permeabilization (0.1% Triton X-100 in 0.1% [w/v] sodium citrate [freshly prepared]) was carried out during 10 min at room temperature. The DNaseI concentration used for the treatment of positive control was 650 U/ml. Slides were evaluated using a Zeiss LSM800 confocal microscope equipped with a 408 nm and 488 nm excitation source for DAPI and FITC staining. Control positive slides were used for determination of the appropriate acquisition settings. Negative control (without terminal transferase) was used to set the minimum fluorescence intensity. Approximately 250 cells were analyzed per replicate with ImageJ software (Image J, Madison, WI, USA). The results were expressed as the percentage of cells with fragmented DNA (**Supplementary Figure 2**).

Alternative immunofluorescence protocol for colocalization of 8-OHdG with H3, TOPO IIα + β and PRDX6

Fixation steps were carried out in different ways to show that localization of the antigens remained unalterable. Two different protocols were tested: (i) fixation with ethanol:acetic acid (1:1) prior to cell smearing on coated slides or (ii) denaturing step with 2.5 mmol/L DTT (10 min 37°C) and subsequent fixation with PFA or ethanol:acetic acid (data not shown; despite maintaining the localization of antigen in the nucleus, the cell morphology changed and the sperm nucleus was seen to be larger and rounder). Once the smears were prepared on ATE coated slides, the rest of the protocol continued as described in the section "Colocalization of 8-OHdG with histone H3, TOPO IIα+β and PRDX6" (**Supplementary Figure 1**).

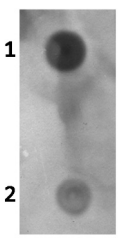

Supplementary Figure 1: Dot blot analysis of histones extracted during human chromatin sperm fractionation. Commercial histones from calf thymus (**1**) and histones extracted after chromatin fractionation (**2**) were subjected to Dot blot with anti-histone H3 antibody.

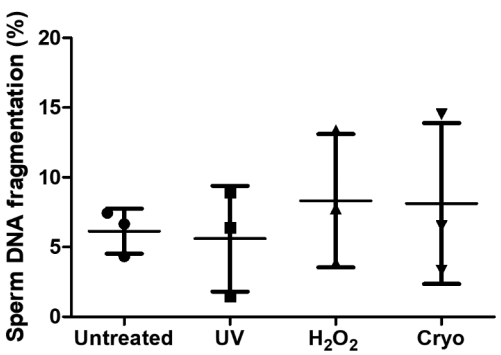

Supplementary Figure 2: Chromatin integrity evaluated by TUNEL assay in human ejaculate after treatments. DNA damage is expressed as the percentage of FITC positive cells (n = 3, at least 250 cells analyzed per replicate, total replicates: 3).

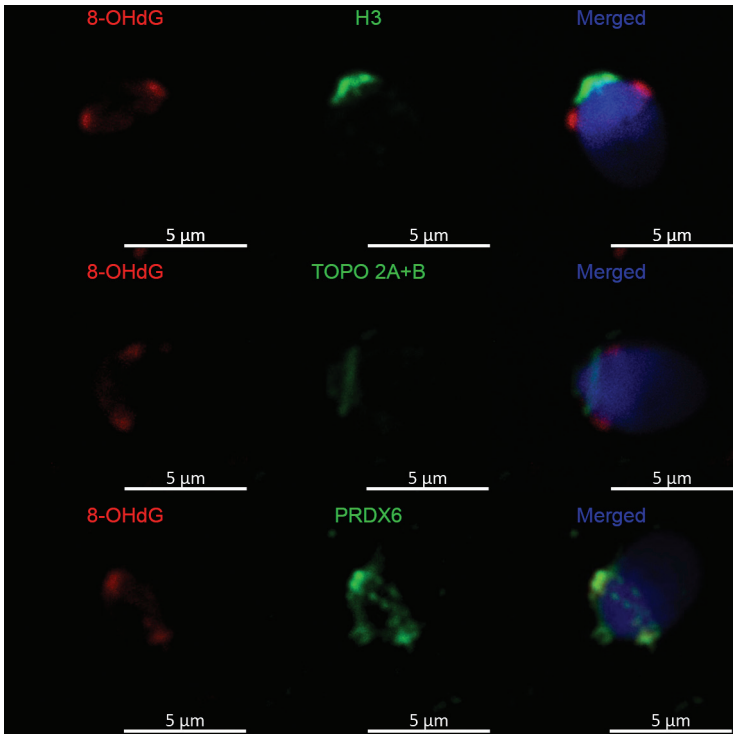

Supplementary Figure 3: Colocalization of 8-OHdG with H3, TOPO IIA+B and PRDX6 in human spermatozoon after oxidative damage using a different fixation and permeation step. Representative confocal images were taken in H_2O_2-oxidized sperm, which were fixed with ethanol:acetic acid; localization of 8-OHdG was revealed, labeled with AlexaFluor®568, appearing in red fluorescence, and distribution of histone H3, TOPO IIA+B, and PRDX6, labeled with AlexaFluor®488, green in color. Cell nuclei were stained with DAPI and appear in blue. Scale bar, 5 µm.